Proc. Natl. Acad. Sci. USA
Vol. 93, pp. 4261–4266, April 1996
Physics

Bond orientational order, molecular motion, and free energy of high-density DNA mesophases

R. PODGORNIK*†, H. H. STREY*‡, K. GAWRISCH§, D. C. RAU‡, A. RUPPRECHT¶, AND V. A. PARSEGIAN*‡‖

*Laboratory of Structural Biology, Division of Computer Research and Technology, ‡Office of the Director, Division of Intramural Research, National Institute of Diabetes and Digestive and Kidney Diseases, §Division of Intramural Clinical and Biological Research, National Institute of Alcohol Abuse and Alcoholism, National Institutes of Health, Bethesda, MD 20892; and ¶Physical Chemistry, Arrhenius Laboratory, University of Stockholm, Stockholm, Sweden

Communicated by David R. Nelson, Lyman Laboratory of Physics, Cambridge, MA, December 11, 1995 (received for review September 15, 1995)

ABSTRACT **By equilibrating condensed DNA arrays against reservoirs of known osmotic stress and examining them with several structural probes, it has been possible to achieve a detailed thermodynamic and structural characterization of the change between two distinct regions on the liquid-crystalline phase diagram: (*i*) a higher density hexagonally packed region with long-range bond orientational order in the plane perpendicular to the average molecular direction and (*ii*) a lower density cholesteric region with fluid-like positional order. X-ray scattering on highly ordered DNA arrays at high density and with the helical axis oriented parallel to the incoming beam showed a sixfold azimuthal modulation of the first-order diffraction peak that reflects the macroscopic bond-orientational order. Transition to the less-dense cholesteric phase through osmotically controlled swelling shows the loss of this bond orientational order, which had been expected from the change in optical birefringence patterns and which is consistent with a rapid onset of molecular positional disorder. This change in order was previously inferred from intermolecular force measurements and is now confirmed by ^{31}P NMR. Controlled reversible swelling and compaction under osmotic stress, spanning a range of densities between ≈120 mg/ml to ≈600 mg/ml, allow measurement of the free-energy changes throughout each phase and at the phase transition, essential information for theories of liquid-crystalline states.**

Double helical DNA has emerged as a remarkably useful material for visualizing liquid-crystalline structures (1) and for measuring the packing energies associated with them. Robust DNA double helices, of almost any monodisperse length from a few base pairs to molecular weights ≈10^9, can be obtained through modern molecular biology methods and can be condensed into highly ordered arrays easily probed by x-ray diffraction. The strong polyelectrolyte interactions between helices can be controlled effectively by type and concentration of the excess electrolytes. The form of the interhelical potential suggests that the lessons learned from concentrated DNA arrays will have broad applications to other seemingly unrelated physical systems, such as their recently noticed similarity to magnetic vortex arrays in type II superconductors (2).

Given the extensive investigations of the physical properties and structure of condensed DNA phases, it is surprising that there has not yet been a comprehensive thermodynamic characterization of DNA mesophases under controlled solution conditions. Following Robinson's (3) seminal observation of a cholesteric-like phase of long DNA *in vitro*, there have appeared several studies detailing the complexity of DNA phase behavior and its relevance for the conditions *in vivo* (1). The sequence of mesophases for short-fragment DNA (146 bp, ≈50-nm nucleosomal DNA) appears to be: isotropic solution → cholesteric → columnar hexagonal → hexagonal (4). With biologically more relevant long-fragment DNA (≈100 nm to ≈1 mm), the sequence of phases is less well delimited and characterized: isotropic solution → ("precholesteric" →) cholesteric → columnar hexagonal → hexagonal crystalline (5). These sequences were obtained on stoichiometric mixtures of DNA, salt, and water where there is often more than one phase present and where neither salt nor water chemical potentials are known.

A separate line of study of the condensed phases of DNA was initiated by Lerman (6) through the polymer- and salt-induced condensation (ψ DNA) and equilibrium sedimentation (7) of DNA solutions. The density of the condensed DNA was shown to depend continuously on the concentration of condensing polymer agent (usually PEG) (8). The use of osmotic stress (9) was built on the realization that the condensing polymer is essentially fully excluded from the DNA phase and that, at equilibrium, the activities of the exchanging water and salt are equal in the DNA and PEG phases (10). Knowing the osmotic pressure (Π) contribution from the excluded polymer, measured by standard procedures as a function of its concentration, means the osmotic pressure of the DNA is also known while all other intensive variables such as pH and the chemical potentials of salt and other small solutes (9–11) are held fixed. Using x-ray scattering to measure the interaxial spacing D between double helices, this method was used successfully to elucidate a $\Pi - D$ dependence for DNA as a function of temperature, salt type, and salt concentration (10, 11). The range of osmotic pressures accessible through this method is substantially larger (especially at high stress) than by the equilibrium sedimentation approach (7).

Because DNA is equilibrated against a vast excess of a polymer and water solution of known chemical potential, it is always in a single phase at thermodynamic equilibrium. This behavior should be contrasted with multiple-phase equilibria that usually emerge from stoichiometric mixtures.

In this work, we combine both the structural and thermodynamic approaches to the condensed DNA phases so that structural and dynamical parameters of DNA packing and ordering (interhelical separation, bond orientational order parameter, ^{31}P-NMR spectra) are all measured concurrently with the free energy and/or its derivatives. We report here the structural and dynamic changes that occur in the DNA concentration region from 120 to 600 mg/ml corresponding to interaxial separations of 25–55 Å. We show that at lower densities (or higher spacings) DNA packing is characterized by short-range positional order, measured by x-ray diffraction, long-range cholesteric order, revealed by optical birefringence, and high mobility of the DNA backbone, inferred from ^{31}P-NMR spectroscopy. At high densities (or small spacings) DNA packing is characterized by short-range positional order and long-range bond orientational order in the plane perpendicular to the average nematic director, revealed by the

The publication costs of this article were defrayed in part by page charge payment. This article must therefore be hereby marked "*advertisement*" in accordance with 18 U.S.C. §1734 solely to indicate this fact.

†On leave from: J. Stefan Institute, Ljubljana, Slovenia.
‖To whom reprint requests should be addressed.

azimuthal profile of the first order x-ray diffraction peak and low mobility of the DNA backbone.

MATERIALS AND METHODS

Wet-spun oriented samples were prepared from calf thymus DNA (Pharmacia) with a molecular weight of $\approx 10^7$ (corresponding to a contour length of ≈ 5 μm or some $\approx 10^2$ persistence lengths) by the described method (12). This spinning allows controlled production of sufficient amounts of highly oriented thin films by spooling DNA fibers that are continuously stretched during precipitation into an aqueous alcohol solution. Films of thickness of ≈ 0.5 mm and surface area between 5 and 10 mm^2 were used.

Unoriented fibers of high molecular weight ($\approx 10^8$ corresponding to ≈ 50 μm or equivalently $\approx 10^3$ persistence lengths) DNA were prepared from whole adult chicken blood (Truslow Farms, Chestertown, MD) as described in McGhee *et al.* (13). This DNA was further purified with three extractions against phenol/chloroform, 50:50 (vol/vol), and once with chloroform alone. DNA was then ethanol-precipitated in sodium acetate, pelleted by centrifugation, washed twice with 70% (vol/vol) ethanol, and dried. This DNA was used in all preparations involving unoriented fibers.

Both oriented and unoriented DNA fibers were equilibrated with various solutions of PEG (M_r 20,000) in 0.5 M NaCl/10 mM Tris/1 mM EDTA, pH 7, in vast excess. Under these conditions, PEG (M_r 20,000) is completely excluded from the DNA phase for concentrations greater than $\approx 7\%$ (wt/wt). The equilibration time was usually from 4 days to a week. Measurements on both orientationally ordered (wet-spun) as well as "powder" samples show that there is essentially no difference in osmotic pressure vs. concentration (interhelical spacing) dependence between the two preparations. The two preparations differ only in the size of the oriented domains.

X-ray diffraction was performed at 20°C with an Enraf–Nonius (Bohemia, NY) fixed-anode FR 590 x-ray generator equipped with image plate detectors. Image plates were read and digitized by a PhosphorImager SI (Molecular Dynamics) and processed with IMAGE version 1.55 program (W. Rasband, National Institutes of Health, Bethesda) that we modified. The geometry of the scattering setup for the oriented thin film is presented in Fig. 1. The position of the first-order diffraction peaks ($r_{1.max}$) is obtained by radially averaging the scattering profile around the direct beam. Angular intensity profiles were taken at the position of the maximum of the first-order diffraction peak and were then Fourier-transformed to extract the bond orientational order parameter C_6, i.e., the sixth-order Fourier coefficient. If there were perfect alignment of the x-ray beam and the average director of the oriented DNA sample,

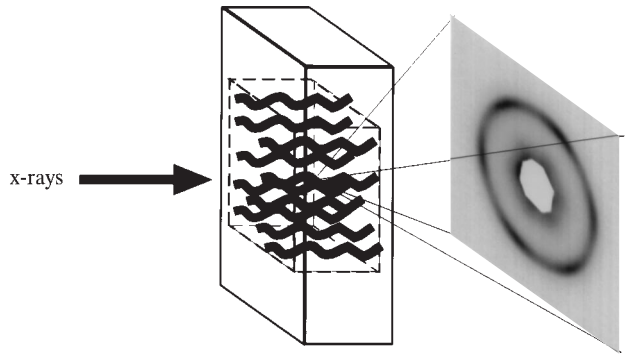

FIG. 1. Schematic representation of the x-ray scattering setup of oriented films. The oriented thin DNA sample is positioned in such a way that the average director points in the direction of the incoming x-ray beam. The PEG solution, providing the osmotic stress, bathes the whole DNA sample.

the angular dependence of the sixfold symmetric scattering function could be Fourier-analyzed in terms of ref. 14 as follows:

$$S(\theta, r_{1.max}) = I_0(r_{1.max}) \left[\frac{1}{2} \sum_{n=1}^{\infty} c_{6n} \cos 6n(\theta - \theta_0) \right] + I_{BG}, \quad [1]$$

where I_{BG} is the background intensity.

Because the orientation was only approximate, there was usually a small C_2 component present in the Fourier-analyzed angular profiles. We have rescaled the value of C_6 to correct for this. We have checked that the C_2 component can be completely removed from the angular diffraction profiles by orienting the sample appropriately.

A weak first-order B-DNA base-stacking reflection at ≈ 3.4 Å was present at all the densities investigated here, precluding any possibility of reorganization within the chains as a function of DNA density.

DNA samples at various densities were sealed between microscope cover glasses and were observed under a microscope [Olympus (New Hyde Park, NY)] equipped with crossed polarizers. The image was digitized and analyzed with IMAGE version 1.55. The "fingerprint" cholesteric pattern (15) with long-fragment DNA was never as regular as is typical of short-fragment DNA. Rather long DNAs achieve oriented domains of much smaller size.

The ^{31}P NMR measurements were performed on a Bruker (Billerica, MA) model MSL-300 spectrometer using a high-power probe with a 5-mm solenoidal sample coil that was doubly tuned for ^{31}P (121.513 MHz) and protons (300.13 MHz). Gated broadband decoupled ^{31}P spectra were observed with a phase-cycled Hahn echo sequence. A delay time between the 90° pulse and 180° pulse of 30 μsec was chosen. Typically, 20,000–80,000 scans with a recycle delay time of 1 sec were accumulated. Exponential linebroadening with a linewidth of 200 Hz was used.

First moments of the NMR spectra (M_1) were calculated according to definitions used in NMR spectroscopy (16) as follows:

$$M_1 = \frac{\int_{-\infty}^{+\infty} |\omega| f(\omega)\, d\omega}{\int_{-\infty}^{+\infty} f(\omega)\, d\omega}, \quad [2]$$

where $f(\omega)$ is the spectral intensity at the frequency ω. The frequency of the center of the spectrum, determined as half height of the integral $\int_{-\infty}^{+\infty} f(\omega)\, d\omega$, was set to zero. In deviation to standard procedures, integration was performed over absolute frequency values $|\omega|$. M_1 defined in this fashion has a maximum for totally immobilized DNA and approaches zero for rapid isotropic tumbling motions.

The measured dependence of the osmotic pressure of the DNA phase on DNA concentration allows one to evaluate the reversible work done at constant temperature, pressure, and chemical potential of salt as the system is brought from an initial (i) to a final (f) configuration. The difference in free energy G is

$$\Delta G = -\int_{V^i}^{V^f} \Pi(V_{DNA})\, dV_{DNA}. \quad [3]$$

The excess or packing energy per unit length of the DNA helix can now be obtained as

$$\frac{\Delta G}{L} = -\sqrt{3} \int_{D_i}^{D_f} \Pi(D)\, DdD, \quad [4]$$

where D is the interhelical spacing assuming the DNA array is at least locally hexagonal. Since the DNA osmotic pressure decays exponentially at small and intermediate values of D, a finite density interval is sufficient to evaluate the above integral to satisfactory accuracy. We have taken D_i corresponding to the concentration 15 mg/ml (data not shown in Fig. 2), which marks the onset of the condensed (anisotropic) DNA phase (17).

Since thermal fluctuations are contributing to the free energy, it is reasonable to express the calculated free energy per unit length, $\Delta G(D)/L$, in its "natural" units of kT per persistence length $\mathcal{L}_p$ (≈500 Å). In these units one can write

$$\frac{(\Delta G(D)/kT)}{L/\mathcal{L}_p} = \frac{\mathcal{L}_p}{\zeta(D)}, \qquad [5]$$

where $\zeta(D)$ is the contour length of DNA associated with kT of packing energy in the condensed phase.

RESULTS

Osmotic Stress Measurements. The dependence of osmotic pressure on the concentration of the unoriented DNA subphase has been investigated in detail (10, 11, 18). The corresponding interhelical spacings were obtained by measuring the first-order x-ray diffraction peak on unoriented DNA samples with the assumption of local hexagonal packing symmetry. This assumption was verified experimentally in the high-density region (I) (Fig. 2) through the existence of weak higher order reflections and now by observing well-developed sixfold symmetric bond orientational order (see *Packing Symmetry*).

Similar measurements were performed on oriented samples that show the same interaxial spacing (or density) dependence on Π as the unoriented samples (see Fig. 2) and thus have the same free energy, within experimental error. There are two distinct regions in the $\Pi - D$ curve. In the high-pressure regime, the interhelical distance does not depend on the salt concentration. The forces between helices in this region were interpreted as resulting from water-mediated structural forces (10). At lower pressures, a sensitivity of D to salt concentration is clearly discernible. The effective decay length for the interhelical interactions, however, is about twice the predicted Debye screening length (19) for salt concentrations < 1.0 M, where electrostatic interactions are not overwhelmed by hydration forces. The two scaling regimes of the osmotic pressure are separated by a narrow crossover region in the $\Pi - D$ curve at about 32–34 Å.

Packing Symmetry. The two regimes in the osmotic pressure curve are also clearly evident in the qualitative characteristics of the x-ray diffraction on oriented samples (Fig. 3). For oriented samples of DNA in the high-osmotic-pressure regime (I), the cross section of the first-order interaxial diffraction peak with the DNA helical axis oriented parallel to the incoming beam is a circular ring with sixfold modulation in the intensity that clearly reflects the sixfold symmetric long-range bond orientational order of the underlying DNA lattice (Fig. 3 *Inset*). Azimuthal modulation of the first-order diffraction peak at close DNA spacings has been observed previously in neutron diffraction studies (20) with fibers of NaDNA and LiDNA at low excess salt content. As the osmotic pressure is lowered, the sixfold modulation of the first-order diffraction peak disappears and is unobservable below the transition, 32–34 Å, region (see Fig. 3 *Inset*) in the $\Pi - D$ curve. For spacings <35 Å, the changes in the sixfold modulation of the diffraction peak were reversible. At larger spacings, however, once the bond orientational order is lost, it cannot be regained by simply increasing the osmotic pressure. The subsequent chain entanglement due to the looser nature of the packing in this low-pressure phase apparently precludes the reestablishment of long-range bond orientational order. The details of the first-order diffraction peak are irretrievably lost leading to a circular powder pattern.

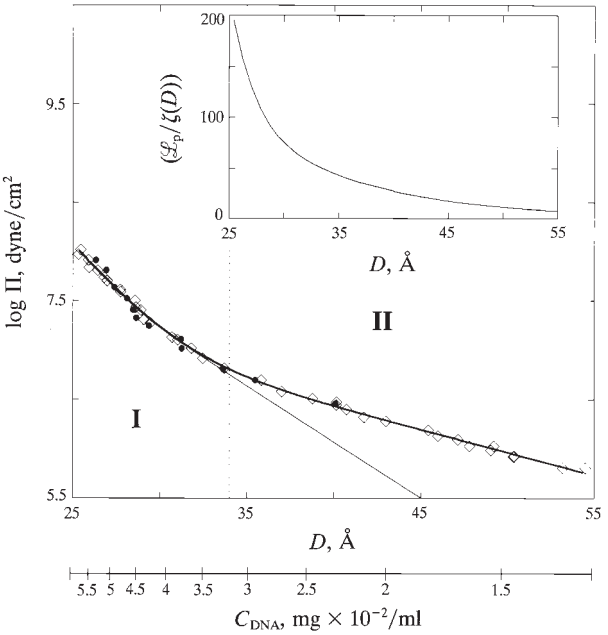

FIG. 2. Osmotic pressure of DNA, stressed by solutions of PEG (M_r 20,000) at different concentrations, as a function of the interhelical spacing for 0.5 M NaCl DNA, for wet-spun, highly oriented DNA (●), and for condensed unoriented DNA (◇). No significant difference between the macroscopically oriented and unoriented samples is observed over the osmotic stress region investigated. The upper continuous curve represents a fit to the experimental data with bare hydration forces at high pressures (region I) and fluctuation enhanced screened Coulombic interactions in the low-pressure region (II), while the lower curve represents a hypothetical osmotic pressure dependence if the underlying forces were a simple sum of bare-hydration and screened-Coulomb interactions, neglecting the contribution from DNA conformational disorder. The dotted vertical region represents the phase boundary between the bond orientationally ordered and the cholesteric phases. A DNA density scale in mg/ml is also given to facilitate comparison with previous work. The inset presents the free energy in units of kT per persistence length (≈500 Å or ≈150 bp). $\mathcal{L}_p/\zeta(D) = 1$ corresponds to one persistence length per kT while 100 corresponds to one-hundredth of a persistence length (or ≈1.5 bp) per kT of interaction energy.

The details of the azimuthal profile of the diffraction pattern were independent of the x-ray beam size up to cross-sectional areas on the order of ≈1 mm². Thus, the bond orientational order appears to be of very long range indeed. The translational order, on the other hand, estimated crudely from the radial linewidth of the first-order diffraction peak (21) and weak higher order reflections (J. Rädler, personal communication), appears to be of a much shorter range, on the order of several lattice spacings.

To quantify this change in orientational bond order, we have measured the azimuthal intensity distribution of the first-order diffraction peak and extracted the corresponding Fourier coefficients shown in Fig. 3. Generally the Fourier spectra showed pronounced peaks for C_n with $n = 0$ and 6, with typically a small, but discernible, additional contribution from C_2, most probably reflecting a slight misorientation between the x-ray beam direction and the average director of the oriented DNA sample. The extracted C_6 coefficients that are also corrected for misalignment show a gradual loss of lateral bond orientational order as the DNA density passes from the high to low osmotic pressure regimes.

The nature of the low osmotic pressure phase can be further ascertained by polarized light microscopy that clearly reveals the existence of a "fingerprint" texture characteristic of a

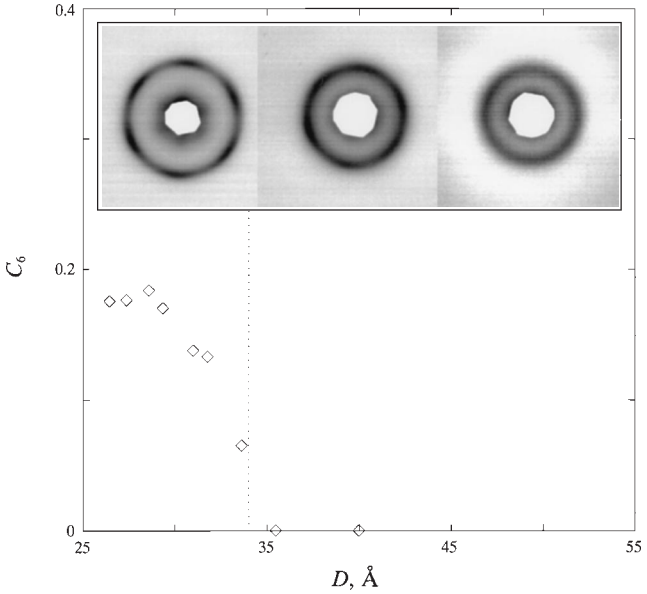

FIG. 3. The dependence of the bond orientational order parameter C_6 on the interaxial spacing in the region of the high-pressure to low-pressure transition. The vanishing of the long-range bond order is clearly visible. Sixfold modulation in the first-order diffraction peak seen directly in the scattering patterns [*Left Inset* to *Right Inset*, log(Π) = 7.80, 7.51, and 6.795 dynes/cm^2 (1 dyne = 10 μN)] gradually weakens and disappears below the transition region (shown by the dotted area) identified in the $\Pi - D$ shown in Fig. 2. The loss of bond orientational order is reversible provided the interhelical spacing does not exceed the transition region (≈35 Å).

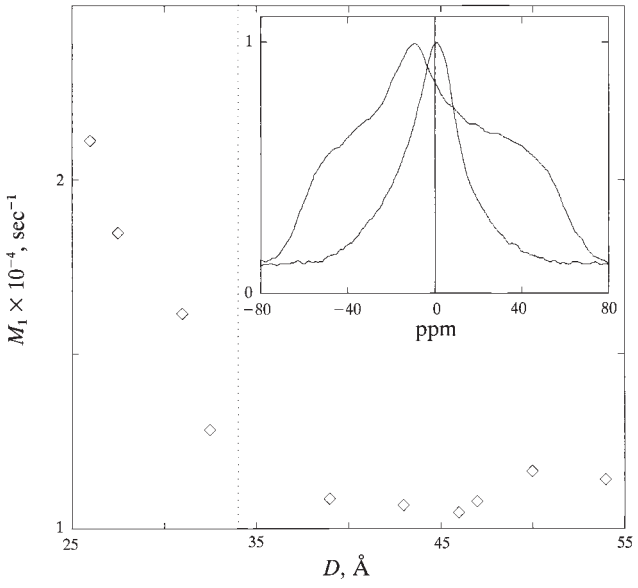

FIG. 4. The first moment M_1 of the ^{31}P-NMR spectra as a function of the interhelical separation D measured on the same (unoriented) samples as with x-ray scattering. There is a qualitative change in the shape of the NMR spectra (see *Inset*) as the system goes through the high-pressure to low-pressure transition region (the dotted area). (*Inset*) Two NMR spectra: at Π = 7.98 dynes/cm^2 corresponding to interhelical spacing of 26 Å (broad spectrum) and at Π = 6.119 dynes/cm^2 corresponding to interhelical spacing of 46 Å (narrow spectrum) and ionic strength 0.5 M NaCl. Much more motional freedom of DNA phosphates is evident at low pressures than high. The change in the behavior of the spectral linewidth at the transition region is quite abrupt.

cholesteric phase (22). Though the pitch of the cholesteric phase varies with density of the DNA phase in the vicinity of the I → II transition, we were unable to quantify this accurately because the orientational domain sizes were generally small. Because of the high molecular weight of the DNA, the samples could not be manipulated by an applied external orienting magnetic field to increase the domain size.

Phosphate Backbone Dynamics. An earlier analysis of the $\Pi - D$ curve suggested that there was a relatively sudden change in lattice fluctuations, inferred from changes in x-ray-scattering peak widths, within the 32–34 Å transition region (11). This change in motion can now be seen very clearly in the ^{31}P-NMR spectra. Fig. 4 *Inset* shows two ^{31}P-NMR spectra—a broad spectrum characteristic of the high pressure regime and a narrow spectrum at low osmotic pressure. Both spectra represent powder patterns in which phosphate groups with different orientation to the magnetic field have different chemical shifts of their resonance signals. Typical principal values of the chemical shift tensor extracted from spectra at high osmotic stress are $\sigma_{xx} \simeq -58$ ppm, $\sigma_{yy} \simeq -4$ ppm, and $\sigma_{zz} \simeq 67$ ppm, measured relative to 85% phosphoric acid as an external standard. This is considerably less than the values measured for completely immobilized dry DNA, $\sigma_{xx} \simeq -83$ ppm, $\sigma_{yy} \simeq -22$ ppm, and $\sigma_{zz} \simeq 110$ ppm (23). The effective tensor of DNA in the high pressure phase shows that phosphate motions are present but quite restricted. In particular, no fast motions (correlation times of 10^{-5} sec or less) around one axis of symmetry take place because such motions would have produced a tensor with axial symmetry.

The ^{31}P-NMR spectra of the low osmotic pressure phase are much narrower, indicating DNA backbone motions of larger amplitude. However, the asymmetry of the resonance signal indicates that DNA motions are anisotropic in this phase too. Moreover, the different asymmetries of the ^{31}P-NMR spectra in both phases hint at different types of motions.

To determine at which D spacing the system changes phases, we plotted the spectral first moment, M_1 Eq. **2**, as a function of D spacing (Fig. 4). M_1 decreases rapidly with increasing D from 25 to 32 Å and remains approximately constant thereafter. The molecules are obviously immobilized to a substantial degree in the high-pressure phase, though M_1 indicates a rapid increase of motional freedom with increasing D (decreasing osmotic stress). In the low-pressure phase, phosphate mobility always appears to be high.

DISCUSSION

Structure and Dynamics. This study, together with earlier measurements of intermolecular forces (10, 11), presents a departure from the usual gravimetric method of sample preparation. By bringing ordered phases into equilibrium with large "reservoirs" of salt-plus-polymer solutions rather than by making stoichiometric mixtures of salt, water, and DNA, it is possible to set all the intensive thermodynamic variables associated with the resulting single liquid-crystalline phase.

These simultaneous measurements of the structure, motion, and thermodynamic functions of DNA phases have focused on high-density DNA phases (with interhelical spacings between about 25 and 55 Å) at one ionic strength (0.5 M NaCl). This density region extends from ≈120 to ≈600 mg/ml. At lower densities there is a transition to a cholesteric phase from one of the (presumably) blue phases (24), while at higher densities there is a transition into a three-dimensional crystal with a simultaneous B → A transition in DNA conformation. For the long-fragment DNA investigated here, the isotropic → anisotropic transition is still quite remote [≈10 mg/ml (17)].

The structural, dynamic, and osmotic stress data presented here are all consistent with the existence of two different DNA phases separated by a transition region at a DNA density of ≈320–360 mg/ml, corresponding to interhelical spacings of ≈32–34 Å. Previous work on short-fragment (146 bp, ≈500 Å long) DNA (4) also gave clear evidence for the existence of a

series of structurally distinct regions as a function of DNA concentration. The transition from a cholesteric to a two-dimensional-hexagonal phase for short-fragment DNA was observed at ≈32 Å. Remarkably the ≈32 Å interaxial spacing is also close to the spacing from which Mn^{2+}– or Co^{3+}–DNA collapses in a first-order transition under osmotic stress (25). Is this a distance at which the details of the chiral double-helical structure come to be sensed in molecular interaction?

What these experiments do not show clearly is the nature and the order of the transition between bond orientationally ordered and cholesteric phases. There is no detectable discontinuity (the accuracy of the measurement of the interhelical spacing in this regime of DNA densities is ≈1 Å) in the Π vs. interaxial separation curve that is seen when DNA makes a clear first-order transition (25, 26). This should not be taken as definitive evidence, however, that the transition is second order. An extremely narrow phase-coexistence window could simply be a property of polymers in liquid-crystalline mesophases (27). The accuracy of the azimuthal scans of the first-order diffraction peak as well as the first moment of the ^{31}P-NMR spectra also precludes a definitive measure of the order of the transition.

Free Energy and Intermolecular Forces. The osmotic stress exerted by the excluded polymer is the rate of change of free energy with change in the amount of solution in the DNA phase—i.e., $\Pi = -\delta G/\delta V_{DNA}$. By integrating the osmotic pressure curve, one thus obtains the change in the system free energy, Eq. 4. In the inset to Fig. 2, we have plotted this free energy as a function of molecular separation. It is given in thermal units of kT per persistence length (see Eq. 5), and spans a wide range of energy scales, from about kT per 2.5 Å at log(Π) ≈8 dynes/cm^2 to about kT per 100 Å at log(Π) ≈6 dynes/cm^2.

Previous work (18) has established that forces in the high-pressure regime are dominated by exponentially decaying hydration interactions with a decay length λ ≈3–4 Å that is basically independent of the ionic strength. In the low-pressure regime, the interaxial spacing dependence on osmotic stress is also exponential, but the effective decay length is about twice the expected Debye decay length (at least for salt concentrations between 0.2 and ≈0.8 M). The enhanced decay length and a rescaling of the strength of the interactions between DNA helices in this regime of DNA densities was shown to be due to the progressive onset of conformational disorder characterized by the fluctuations in the mean position of the molecules along the average director (18, 28) and deduced from the width of the interhelical x-ray scattering peaks. The switch between fluctuation enhanced forces and bare potentials was not found to be gradual, but rather quite abrupt as the DNA density passed the ≈340 mg/ml limit (11), correlating nicely with emergence of longitudinal order between helices seen in the studies of Livolant and coworkers (4) on short fragment DNA, as well as with the onset of lateral bond orientational order and broadening of the phosphate NMR spectrum reported here.

The fluctuation-enhanced effective interactions observed in DNA arrays have the same origin as the effective interactions in smectic arrays. They are due to the interplay between conformational fluctuations and bare short-range potentials (19). The clearly emerging enhancement of electrostatic decay length to about twice the Debye length, not yet so easily seen in lipid bilayer smectic arrays, could be connected with the different dimensionalities of the two systems (two-dimensional periodicity vs. one-dimensional periodicity).

Perspectives and Directions. Molecular interactions in DNA arrays, extracted from the measured osmotic pressure of the array, are expected (11) to vary with the interaxial spacing D as $\approx K_0(D/\lambda)$, where $K_0(x)$ is the modified Bessel function with asymptotic behavior $K_0(x) \approx (\pi/2x)^{1/2} e^{-x}$, with a decay length λ dependent on the salt concentration (18). In this respect, as noted by Nelson (2), the interactions between helices in condensed DNA mesophases are formally and surprisingly closely related to the interactions between magnetic vortex lines in flux-line lattices of high-T_c superconductors that, apart from the lack of hard core repulsions, share the same form of interaction potential.

The existence of a line (polymer) hexatic phase, intermediate between a line crystal and a line liquid, was hypothesized by Marchetti and Nelson (29) specifically for the case of magnetic flux-line lattices. It appears that the bond-ordered DNA phase (region I) described above is perhaps this type of intermediate phase. The transition from a line hexatic phase in DNA into one of the possible less ordered phases is complicated by the presence of chiral coupling in the molecular interactions at lower densities, leading to the cholesteric, not a line liquid, phase. This fact alone warrants closer scrutiny as one would perhaps expect that the cholesteric coupling would prevail at smaller, not larger, interaxial separations, where the molecular details of neighboring molecules are more easily felt. It was hypothesized recently that the absence of cholesteric organization in chiral polymers at large densities could be viewed as a type of Meissner effect, where the cholesteric pitch instead of the magnetic field is expelled from the sample (D. R. Nelson and R. D. Kamien, personal communication).

The occurrence of a line hexatic phase between the cholesteric and the crystalline (A-form DNA) phases makes it difficult to compare the experimental findings directly with existing theoretical predictions. On the other hand, there are no theoretical predictions for the structure function or hexatic order parameter behavior in the line hexatic phase as it has not been observed before. Its existence introduces a new possible scenario into the melting sequence of ordered (chiral) polyelectrolyte arrays. We hope that the reality of these phases and the possibility of measuring their properties will stimulate further theoretical efforts to understand their unique behavior.

To say that DNA provides an opportunity to learn about liquid crystals is not to say that it has already given clear answers to basic questions. What is the nature of the transition from a phase with well developed sixfold symmetric bond orientational order to a skewed, cholesteric phase when the molecules are allowed to move apart? Why does this change in symmetry couple with the molecular motions that cause extra interaxial separation (11)? What is the nature of molecular packing in the long polymer cholesteric phase compared to the more common twisted nematic phases of shorter molecules? What is the effect of the polymer length on the sequence of high density mesophases? These combined structural studies (4), osmotic stress measurements of free energies, and x-ray and NMR probes of molecular disorder and motion now provide a direction and an opportunity for further development of systematic theoretical analyses.

R.P. acknowledges the support of the Ministry of Science and Technology of Slovenia through a traveling grant within the contract J1–6168-381–94. H.H.S. thanks the Deutsche Forschungsgemeinschaft for a research scholarship.

1. Livolant, F. (1991) *Physica A* **176,** 117–137.
2. Nelson, D. R. (1995) in *Observation, Prediction and Simulation of Phase Transitions in Complex Fluids*, eds. Baus, M., *et al.* (Kluwer, Dordrecht, The Netherlands), pp. 293–335.
3. Robinson, C. (1961) *Tetrahedron* **13,** 219–234.
4. Durand, D., Doucet, J. & Livolant, F. (1992) *J. Phys. II* **2,** 1769–1783.
5. Livolant, F. (1987) *J. Phys. (Paris)* **48,** 1051–1066.
6. Lerman, S. (1971) *Proc. Natl. Acad. Sci. USA* **68,** 1886–1890.
7. Brian, A. A., Frisch, H. L. & Lerman, S. (1981) *Biopolymer* **20,** 1305–1328.

8. Yevdokimov, Yu.M., Skuridin, S. G. & Salyanov, V. I. (1988) *Liq. Cryst.* **3,** 1443–1459.
9. Parsegian, V. A., Rand, R. P., Fuller, N. L. & Rau, D. C. (1986) *Methods Enzymol.* **127,** 400–416.
10. Rau, D. C., Lee, B. K. & Parsegian, V. A. (1984) *Proc. Natl. Acad. Sci. USA* **81,** 2615–2621.
11. Podgornik, R., Rau, D. C. & Parsegian, V. A. (1994) *Biophys. J.* **66,** 962–971.
12. Rupprecht, A., (1966) *Acta Chem. Scan.* **2,** 477.
13. McGhee, J. D., Wood, W. I., Dolan, M., Engel, J. D. & Felsenfeld, G. (1981) *Cell* **27,** 45–55.
14. Brock, J. D., (1991) in *Bond-Orientational Order in Condensed Matter Systems*, ed. Strandburg, K. J. (Springer, Berlin), pp. 1–29.
15. Podgornik, R., Strey, H. H., Rau, D. C. & Parsegian, V. A. (1995) *Biophys. Chem.* **57,** 111–121.
16. Davis, J. H. (1983) *Biochim. Biophys. Acta* **737,** 117–171.
17. Merchant, K. (1993) Ph.D. thesis (Florida State Univ., Tallahassee).
18. Podgornik, R., Rau, D. C. & Parsegian, V. A. (1989) *Macromolecules* **22,** 1780–1786.
19. Evans, E. A. & Parsegian, V. A. (1986) *Proc. Natl. Acad. Sci. USA* **83,** 7132–7135.
20. Grimm, H. & Rupprecht, A. (1991) *Physica B* **174,** 291–299.
21. Chaikin, P. M. & Lubensky, T. C. (1995) *Principles of Condensed Matter Physics* (Cambridge Univ. Press, Cambridge, U.K.).
22. Leforestier, A. & Livolant, F. (1991) *Biophys. J.* **65,** 56–72.
23. Shindo, H. (1985) *Adv. Biophys.* **20,** 39–57.
24. Leforestier, A. & Livolant, F. (1994) *Liq. Cryst.* **17,** 651.
25. Rau, D. C. & Parsegian, V. A. (1992) *Biophys. J.* **61,** 246–259.
26. Rau, D. C. & Parsegian, V. A. (1992) *Biophys. J.* **61,** 260–271.
27. Gupta, A. M. & Edwards, S. F. (1993) *J. Chem. Phys.* **98,** 1588–1596.
28. Podgornik, R. & Parsegian, V. A. (1990) *Macromolecules* **23,** 2265–2269.
30. Marchetti, M. C. & Nelson, D. R. (1990) *Phys. Rev. B* **41,** 1910–1920.